PAPER

Check for updates

Janus membranes with asymmetric cellular adhesion behaviors for regenerating eardrum perforation†

Zhili Zhang,‡[a] Jin-Bo Li,‡[b] Xu Li,[c] Cheng-Ye Zhu,[c] Liujie Ren,*[d] Xiao-Jun Huang,*[c] Jian Wu,*[b] Jian Ji 🆔[c] and Zhi-Kang Xu 🆔*[c]

The tympanic membrane plays an important role in the human hearing system, which is easily perforated under unfavorable conditions, leading to loss of hearing and otitis media. Many autologous materials and artificial materials have been used to repair a perforated tympanic membrane, but these materials sometimes can cause severe hearing loss because of their adhesion to the ossicle during the healing process and the postoperative process. Herein, we report Janus membranes with asymmetric cellular adhesion behaviors for regenerating the eardrum. These Janus membranes are constructed by co-depositing a tannic acid (TA)/3-aminopropyltriethoxysilane (APTES) coating on one surface of the polypropylene microfiltration membrane. Cellular experiments indicate that the Janus membranes have good biocompatibility and asymmetric cellular adhesion properties. The repair of the tympanic membrane perforation experiment and laser Doppler vibrometer (LDV) measurements prove that the hydrophilic surface of Janus membranes repairs perforated eardrums, and meanwhile the hydrophobic surface can avoid adhering to the inner ear tissue for reducing hearing loss. The Janus membranes have good prospects in the treatment of tympanic membrane perforation.

1 Introduction

The tympanic membrane (TM) is also called the eardrum. TM perforation is a common disease caused by trauma or otitis media in the clinic, which can lead to recurrent episodes of otitis media, hearing loss, and serious headache.[1–5] The mild TM perforation can heal automatically; however, the severe TM perforation needs to be repaired with the help of surgery to improve hearing and reduce the frequency of otitis media.[6–8] The traditional TM regeneration surgery has used autogenous materials such as temporal muscle fascia serving as the scaffold for the regeneration of TM tissue to repair the TM. However, this treatment is usually complex, expensive, and time-consuming,

and in particular, creates a wound in the body to obtain autogenous materials. It is an urgent challenge to exploit artificial materials with the development of ear endoscopy technology and the demand for minimally invasive surgery for doctors and patients.[9,10]

Many artificial materials are emerging as substitutes for TM regeneration due to their good biocompatibility, moderate thickness, transparency, and low cost.[11] For example, He *et al.* used gel foam to repair TM perforation, the healing rate was higher and the average healing time was shorter than for spontaneous healing.[12] Catalani *et al.* also applied an electrospun scaffold to repair the TM by mimicking the extracellular matrix. The repaired TMs are smoother and more elastic than the self-healing ones.[13] However, cells on the side close to the inner ear tend to partially adhere to the ossicle during the process of tympanic membrane repair, which is not conducive to the growth of the tympanic membrane and the normal recovery of the ear function. Therefore, it is of great significance to construct new materials with single-sided cell growth for tympanic membrane repair.[14–19]

Janus membranes have contrasting properties on two sides, which have potential in many applications such as water/oil separation,[20] desalination,[21] and emulsification.[22] This Janus property could also be used in tissue repair. Multifunctional polymers with switchable adhesion and stable antiswelling properties in a wet environment are good candidates for precisely and

[a] *Department of Otorhinolaryngology Head and Neck Surgery, The first affiliated hospital of Zhejiang University School of Medicine, Hangzhou 310003, China*

[b] *Department of Chemistry, Zhejiang University, Hangzhou 310027, China. E-mail: jianwu@zju.edu.cn*

[c] *MOE Key Laboratory of Macromolecular Synthesis and Functionalization, and Key Laboratory of Adsorption and Separation Materials & Technologies of Zhejiang Province, Department of Polymer Science and Engineering, Zhejiang University, Hangzhou 310027, China. E-mail: xuzk@zju.edu.cn, hxjzxh@zju.edu.cn*

[d] *Department of FPRS, Eye & ENT Hospital of Fudan University, Shanghai 200031, China. E-mail: renliujie@fudan.edu.cn*

† Electronic supplementary information (ESI) available. See DOI: 10.1039/d1tb02418c

‡ These authors contributed equally to this work.

This journal is © The Royal Society of Chemistry 2022

J. Mater. Chem. B, 2022, **10**, 2719–2727 | 2719
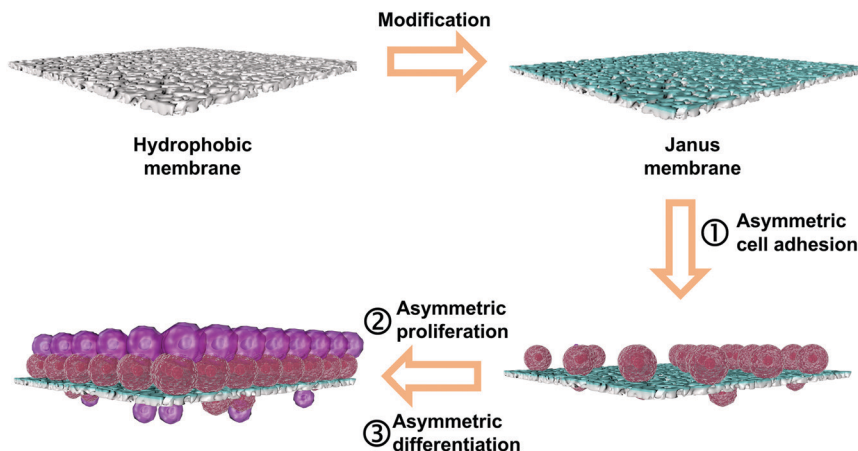
Scheme 1 Schematic illustration for the fabrication process and asymmetric cellular behavior of the Janus membrane.

conveniently monitoring human health.[23–25] Liu et al. studied the wet adhesion of Janus hydrogels with carboxyl and neutralized carboxyl sides for internal tissue repair and preventing the post-operative adhesion.[26] Hwang et al. prepared Janus membranes from chitin nanofibers for bone regeneration and suppressing the migration of the soft tissue.[27] Herein, we report Janus membranes with opposite wettability for the regeneration of the TM. As described in Scheme 1, in our case, the hydrophilic side of the microfiltration membranes is used as a scaffold for regeneration of the TM and the hydrophobic side as the anti-adhesive surface to avoid postoperative adhesion. These Janus membranes were fabricated from polypropylene microfiltration membranes co-deposited with tannic acid (TA) and 3-aminopropyltri-ethoxysilane (APTES). The as-prepared Janus membranes have several characteristics, including (i) the membrane surface is highly biocompatible and non-toxic, avoiding killing of cells;[28–30] (ii) the different wettability of two sides results in asymmetric cellular behaviors, avoiding the adherence of the repair materials onto the ossicle; and (iii) the hydrophilic side can heal TM perforation, lowering the infection rate and recovering audibility.

2 Experimental

2.1 Experimental animal

Female guinea pigs (average body weight 250 ± 10 g) were purchased from the Zhejiang Chinese Medical University Laboratory Animal Research Center. Animal experiments were conducted as per the Guidelines of the Zhejiang University Laboratory Animal Center for the care and use of laboratory animals and were approved by the Animal Care and Use Committee of the Medical School, Zhejiang University. The grafted mice were allowed to survive for 4 weeks before the eardrum tissues were harvested.

2.2 Materials and chemicals

A polypropylene microfiltration membrane (PPMM) with an average pore size of 0.2 μm and a diameter of 2.5 cm was obtained from Membrana GmbH (Germany). The samples were immersed in acetone to remove absorbed impurities and then dried in a vacuum oven at room temperature. Tannic acid (TA)

and 3-aminopropyltriethoxysilane (APTES) were provided by Aladdin (China). Sodium phosphate dibasic and fluorescein were obtained from Macklin Biochemical Co., Ltd. (China). Sodium hydroxide, ethanol, D_2O and acetone were purchased from Sinopharm Chemical Reagent Co., Ltd. N-Propylamine was purchased from Saan Chemical Technology (Shanghai) Co., Ltd. Hematoxylin and eosin were purchased from Thermo Fisher Scientific Co., Ltd. (China). Isoflurane was obtained from RWD Life Science Co., Ltd. (China). DMEM medium was purchased from Cienry Biotech Co., Ltd. (China), and fetal bovine serum (FBS) was purchased from Tianhang Biotechnology Co., Ltd. (China). 3-(4,5-Dimethyl-2-thiazolyl)-2,5-diphenyl-2-H-tetra-zolium bromide (MTT) was bought from Beijing Solarbio Science & Technology Co., Ltd. (China). Calcein AM was purchased from Beyotime Biotechnology Co., Ltd. (China).

2.3 Preparation of Janus membranes with various thicknesses of the hydrophilic layer

Both TA and APTES were dissolved in phosphate-buffered saline (25 mM, pH = 12.5) with a concentration of 2 mg L^{-1} and 12 mg L^{-1}, respectively. PPMM samples were pre-wetted by ethanol for 30 s. The residual ethanol on the membrane surface was removed by filter paper. Then, the membrane was floated on the solution surface of TA/APTES at room temperature (Scheme S1, ESI†). After 15 min and 30 min, the deposited membrane was washed with deionized water and dried in a vacuum oven at room temperature.

2.4 Thickness characterization of the hydrophilic layer of the membrane

The prepared membrane was dipped into a water solution containing sodium fluorescein (0.1 mg mL^{-1}) for 1 min at room temperature. After removing the excess water on the surface of the membrane with filter paper, the membrane was fixed in the test position of a laser scanning confocal microscope (LSCM, ZeissLSM780, Germany). The thickness of the luminous portion was measured under the excitation of a laser (wavelength = 488 nm) to obtain three-dimensional computerized tomography scan images of the membrane.

2.5 Other characterization studies

The surface morphologies of the membrane were observed by field emission scanning electron microscopy (FESEM, Hitachi, S4800, Japan). The chemical structures of the membrane were analyzed by Fourier transform infrared spectrometry (FT-IR/ATR, Nicolet 6700, USA) equipped with an ATR accessory (ZnSe crystal, $45°$) and X-ray photoelectron spectrometry (XPS, PerkinElmer, USA) with Al Kα excitation radiation (1486.6 eV), respectively. ^{13}C NMR spectra were recorded on an Agilent (600 MHz DD2) NMR instrument using D_2O as the solvent at room temperature. The surface wettability was indicated by the water contact angles using a drop Meter A-200 contact angle system (MAIST Vision Inspection & Measurement Co. Ltd, China). The surface charge of the membrane was measured using an electrokinetic analyzer (SurPASS Anton Paar GmbH, Austria). UV-vis absorption of the solutions was measured using an ultraviolet spectrophotometer (UV 2450, Shimadzu, Japan).

2.6 Cell adhesion measurements of the membrane

The membrane with a diameter of 2.5 cm was fixed on a homemade device. An ultraviolet lamp was used to irradiate the front and back of the membrane for 30 min to kill the remaining bacteria in the membrane, and the membrane was placed in a six-well plate. Then the NIH-3T3 cell suspension with a cell density of $50\,000$ mL^{-1} was added to a six-well plate at a volume of 3 mL per well and placed in an incubator with 5% CO_2 at 37 °C for 24 h.

Calcein AM was diluted to a working concentration using a DMEM medium. After that, the medium in the orifice plate was sucked out and replaced with a DMEM medium containing calcein AM. After incubation for 30 min, the medium was sucked out, and the membrane was washed three times with PBS. Then the membrane was replaced in a blank well plate, and the cell adhesion was observed under a fluorescence microscope (Olympus IX81, Japan).

2.7 Cytotoxicity measurements of material extracted liquid

Cytotoxicity of the membrane to the cell was assessed by extracting the membrane with the culture medium and conducting the 3-(4,5-dimethyl-2-thiazolyl)-2,5-diphenyl-2-H-tetrazolium bromide (MTT) assay in the presence of the extract liquids. 4.9 cm^2 of the membrane was immersed in the culture medium containing 2.5 mL of DMEM at 37 °C for two days, and then the main part of the toxic components can be extracted out. The lixivium was then diluted to one-half and one-quarter of the original concentration, respectively.

An NIH-3T3 cell suspension was prepared and NIH-3T3 cells too were incubated in 96-well plates with 5000 cells per well for 20 h to allow cells to attach to the wall. Then the cell culture medium in the 96-well plate was replaced with membrane leaching solution and cultured for 48 h. 5 mL DMEM medium containing 10% FBS was added to 1 mL 5 mg mL^{-1} MTT PBS solution. The membrane leaching solution was removed from the well plate, and 120 µL prepared medium containing MTT was added to each well and reacted for 3 h. Purple crystals could be seen at the bottom of the well plate. After carefully draining the liquid from the well plate, 150 µL DMSO was added to each well. The well plate was put into a microplate reader, and the absorbance of each well was measured at 490 nm and 570 nm after shaking for 5 minutes using a microplate reader (MODEL 550, Bio Rad, USA). Cell viability was represented by a proportion of the absorbance value of the blank group in the same culture medium.

2.8 Animal surgery

Animals were divided into 4 groups, the tympanostomy group, and tympanoplasty groups with 3 species of grafts. The surgical procedure for TM perforation was followed as previously reported. Briefly, the guinea pigs were anesthetized with isoflurane (RWD Life Science, San Diego, California). The area of tympanostomy was about 40–50% of the area of the TM. The myringoplasty was performed immediately after the tympanostomy. Tissues, including the hydrophilic layer of the Janus membranes, the hydrophobic layer of the Janus membranes, and the autologous fascia, with appropriate size were taken as TM repair materials and completely sealed at the borehole to complete tympanoplasty. Endoscopic examination was performed to record the incidence of natural healing, infection, and graft detachment. At 0, 2 and 4 weeks after the surgery, the guinea pigs were sacrificed, and the tissues were collected for histological analysis by H&E staining or a laser Doppler vibrometer.

2.9 Laser Doppler vibrometer (LDV) measurements of TM umbo vibration

TM vibration was measured by LDV. A plastic tape (area 0.25 mm^2, consisting of 50 µm diameter reflective polystyrene microbeads, 3 M, USA) was carefully attached to the TM umbo. The beads should not affect the TM vibration due to their small size and mass. The specimen was placed on a flat plate, with the ear canal facing upwards. A microphone probe (ER-7C, Etymotic Research, USA; sensitivity: 20 Pa V^{-1}) was inserted into the ear canal, about 2 mm from the TM, to measure the sound pressure. The TM umbo velocity was measured on a laser Doppler vibrometer (LDV, CLV-2534, Polytec, Germany; sensitivity: 2 mm s^{-1} V^{-1}), equipped with a dissecting microscope. The laser beam generated by the LDV was roughly perpendicular to the TM. For acoustic stimulations, pure tone sounds were generated by a loudspeaker, driven by signals generated by a signal generator (NI 9263 analog output modules, National Instruments, USA) and amplified by a power amplifier (B&K type 2718, Denmark). Thirty-one frequencies ranging from 250 to 16 k Hz were measured (5 points per octave). To get a better signal-to-noise (SNR) ratio, the stimulus sound was controlled to be about $80 \sim 85$ SPL (by adjusting the amplitude of the output signal). During the measurements, the vibration and sound pressure signals were simultaneously recorded on a data acquisition device (NI 9234, sampling rate 51.2 kHz, National Instruments, USA). An in-house MATLAB program was adopted to control the measurement procedure. The fast Fourier transform (FFT) algorithm was used to process the acquired time-series signals to obtain the amplitude of the sound pressure and umbo velocity.

This journal is © The Royal Society of Chemistry 2022

J. Mater. Chem. B, 2022, **10**, 2719–2727 | **2721**

2.10 Statistics

Qualitative data were presented through relative values. The chi-square test was conducted to analyze relative values of different groups, followed by a partition of chi-square. All data analyses were performed using SPSS version 18 (PASW Statistics for Windows, Chicago: SPSS Inc.). A two-tailed P value of <0.05 was considered statistically significant.

3 Results and discussion

3.1 Surface chemistry, surface morphology, and wettability of Janus membranes

The mussel-inspired catechol chemistry and the single-sided deposition strategy offer great prospects for preparing Janus membranes. In this work, we conducted a single-sided tannic acid/3-aminopropyltriethoxysilane (TA/APTES) codeposition to fabricate Janus membranes with asymmetric wettability. TA was oxidized to quinone derivatives in basic solution and APTES was hydrolyzed in aqueous solution. The oxidized and hydrolyzed chemicals condensed to form cross-linked networks *via* Michael addition and Schiff-base reactions (Scheme S2, ESI†). The formed networks modified the polypropylene membrane from hydrophobic to hydrophilic. It can be seen that the membrane surface becomes more and more hydrophilic with the prolongation of the deposition time. Therefore, the hydrophilization depth of the prepared Janus membranes increases with the extension of the single-sided deposition time (Fig. S1, ESI†). The as-prepared Janus membranes with a hydrophilization depth of 7 μm and 22 μm are named JMs-7

Fig. 1 Chemical analysis and surface wettability of the membrane surfaces. (A) High-resolution of N1S and O1S of JMs-7. (B) High-resolution of N1S and O1S of JMs-22. (C) Digital pictures of water drops on Janus membranes with different hydrophilization depths.

2722 | *J. Mater. Chem. B*, 2022, **10**, 2719–2727

This journal is © The Royal Society of Chemistry 2022

and JMs-22, respectively. Since the deposited networks are at the nanometer level, the morphology of the modified membrane surface has not changed significantly (Fig. S2, ESI†). However, the asymmetric chemistries can be confirmed by FT-IR/ATR and XPS for our Janus membranes. On the hydrophilic side, a new characteristic absorption peak appeared at 1097 cm^{-1} and 1608 cm^{-1}, corresponding to the antisymmetric stretching vibration of Si–O–Si and benzene ring vibration. A new characteristic absorption peak also could be seen at 1730 cm^{-1}, which was related to the vibration of the carbon–oxygen double bond of tannic acid (Fig. S3, ESI†). The binding energies of O1s, N1s, Si2s, and Si2p were found on the deposited side of the Janus membranes. However, the undeposited side only shows a C1s peak and a small O1s peak (Fig. S4, ESI†). The reaction between TA and APTES was proved by NMR and XPS. Fig. 1A and B shows that the nitrogen peak can be resolved into N1 (401.5 eV) and N2 (398.5 eV), which are due to C=N and C–NH, respectively. Since the solution becomes turbid immediately after mixing TA and APTES aqueous solutions, we selected n-propylamine as a simulant molecule for APTES to conduct ^{13}C NMR measurements with results shown in Fig. S5 (ESI†). New peaks of about 150 and 60 ppm in the TA/n-propylamine spectrum are attributed to the formation of C=N and C–NH, suggesting the reaction between TA and n-propylamine.[31] These results prove that TA/APTES crosslinked networks are successfully modified on the membrane surface facing the deposition solution to form Janus wettability. The binding energy peaks of 398.78 eV and 532.40 eV can be assigned to –NH$_3$ and –OH groups in the deposited networks on the membrane surfaces (Fig. 1A and B), respectively. In addition, due to the combination of amino groups and the ionized of phenolic hydroxyl groups, the deposited side of the Janus membranes show a higher absolute values of surface charge than the original membrane in pH, which is equal to 5 or 10 (Fig. S6, ESI†). The surface chemical groups have a significant impact on cell adhesion, proliferation, and differentiation. It is well recognized that those –NH$_3$ and –OH groups play an important role in tissue engineering. The scaffolds with these groups were found to enhance the interactions between cells and biomaterial surfaces and thus promote the expression of cell behavior.[32] The

deposited side of our Janus membranes becomes hydrophilic (Fig. 1C). The time-dependent water contact angle also shows this property (Fig. S7, ESI†). For JMs-22, the initial water contact angle is about 45°, which is expected to be beneficial for cell adhesion.[33]

3.2 Cellular attachment and cytotoxicity of the Janus membranes

The main purpose of the implanted scaffolds is to provide a suitable basis for cell proliferation and tissue growth and the cellular attachment to scaffolds is an important prerequisite for successful transplantation of biomaterials and recovery of body function in tissue engineering.[34,35] The wettability and chemistry of the biomaterial surface play an important role in cell adhesion.[36,37] Fig. 2A exhibits the number and the ratio of cells attached to the two membrane surfaces. For the nascent hydrophobic membrane, the attached cell is low and there is no obvious difference in the cell numbers on the two surfaces. For the Janus membranes, the number of cells attached to the hydrophilic surface is higher than those attached to the hydrophobic one. Furthermore, the cell adhesion ratio of JMs-22 is higher than that of JMs-7. These results may be because the hydrophilic groups of co-deposited TA/APTES coatings are beneficial for adsorbing adhesive proteins, which cause cells to attach to the membrane surface. The difference between the number of adherent cells of JMs-22 and JMs-7 is ascribed to the wettability and chemical properties of the Janus membranes. The adsorption of cell adhesive serum proteins, such as fibronectin and vitronectin, plays a critical role in cell adhesion to the scaffold. Superhydrophilic surfaces with a tightly bound water layer prevent interaction between surface and cell adhesive serum proteins. On more hydrophobic surfaces, albumin adsorbed more strongly and thus cell adhesive proteins could not displace it. Neither could cells adhere on those hydrophobic surfaces. However, on the surfaces with moderate wettability, albumin is easily replaced by cell adhesive proteins and cells adhere well on relatively hydrophilic surfaces. Fig. 2B depicts the cytotoxicity effects of the leaching liquids of the nascent membranes, JMs-7 and JMs-22 on cells evaluated by MTT assay. Compared to the culture medium, all lixivia of the membranes do not exhibit obvious cytotoxicity.
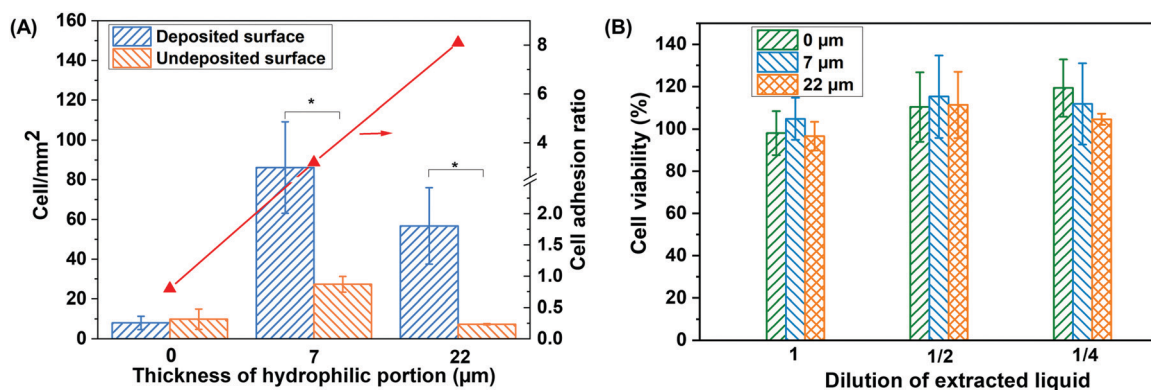

Fig. 2 Cellular adhesion and cytotoxicity of the studied membranes. (A) Number and ratio of the cells attached to co-deposited and undeposited surfaces of Janus membranes with different hydrophilization depths. Significance ($p < 0.5$) is suggested by the asterisk (*). (B) Cytotoxicity analysis of NIH-3T3 that survived in those membrane extract liquids using MTT assay.

This journal is © The Royal Society of Chemistry 2022

J. Mater. Chem. B, 2022, 10, 2719–2727 | 2723

The cell viabilities of original lixivia are in the range of 96.6–104.8%. The double diluted stock solution and the quadruple diluted stock solution show a range of 110.3–115.2% and 104.6–119.3% in cell viability, respectively. The Janus membranes with different hydrophilization depths have no appreciable difference. We therefore choose JMs-22 as the grafted material for TM perforation repair due to the appropriate wettability of the co-deposited surface and the higher cell adhesion ratio.

3.3 *In vivo* experiment and histological examination

We recorded the survival, the death, the infectious, the successfully repaired, and the detached numbers of cells. We also counted the valid success (healing rate), the infection, and the detachment rates during the *in vivo* experiments (Fig. 3). It can be seen that on the hydrophilic surface of JMs-22, the healing rate is up to 77%, with 30 healing cases and 9 cases showing material detachment from the body among 48 initial ears. This result is like 78% of the autologous fascia group. On the hydrophobic surface, there are 46 initial ears for repair, which ultimately show a healing rate of only 8% with 3 healing cases and 35 cases detaching the Janus membrane from the body. It suggests a favorable healing performance of JMs-22, providing tissue cell growth-support by the hydrophilic surface and anti-adhesion properties by the hydrophobic surface, which is expected in clinical practice. In the spontaneous healing group, the total success rate is about 73%, which is slightly lower than the hydrophilic surface of JMs-22 and the autologous fascia group. Though the healing rate of the spontaneous healing group is as high as 73%, the infection rate is higher than the other groups. It assumes that largely infectious or dead guinea pigs are excluded. At the same time, considering the strong self-repair ability of guinea pigs, the healing rate is for reference only, which needs to be comprehensively evaluated in combination with mortality and infection rate.

There is no statistical significance ($P > 0.05$) in the healing rate, infection rate and detachment rate between the autologous fascia group and the hydrophilic surface of JMs-22. However, there is statistical significance between the hydrophobic surface and the hydrophilic surface of JMs-22 in the detachment rate ($P < 0.05$). The detachment rate of the hydrophobic surface is far higher than that of the hydrophilic surface. It could be a good proof of preventing adhesion for the hydrophobic surface of the Janus membrane.

According to literatures, the time interval between tympanostomy and myringoplasty varied differently.[38–41] Some believed long intervals as tympanoplasty was used for animal models of otitis media, while some believed immediate tympanoplasty was reasonable with sufficient controls. As the feasibility and hydrophilicity of JMs-22 were the key points in this paper, we preferred an immediate surgery.

A high detachment rate can testify to low adhesion rate. There is statistical significance between the hydrophobic surface and the hydrophilic surface of JMs-22 in the detachment rate, which shows $P < 0.05$ (Fig. 3). There are only 3 cases in which the Janus membrane does not fall off in the hydrophobic surface. The detachment rate is far higher for the hydrophobic surface than for the hydrophilic surface. Clinically, TM repair is frequently accompanied by tympanic adhesion. In addition, patients with otitis media or tympanic perforation often have eustachian tube dysfunction, even after surgery of myringoplasty, which cannot be easily managed by autologous fascia repairment and could lead to reperforation or adhesion. Attempts have been made to prevent adhesion by using perichondrium or some drugs, while the long-term effect tends to be unsatisfactory. Tympanic adhesion, therefore, is a great challenge for ear surgeons to some extent.[16–19] In this context, the hydrophobic and the anti-adhesion properties to the tissue of JMs-22 are becoming increasingly important. In this study, the Janus membrane was devised for TM perforation repair using the inner-transplant method. The hydrophilic surface obtains a similar success rate in TM perforation healing to clinical autograft muscle fascia, indicating the reliability of the Janus membrane. With the hydrophobic surface attached to tissue, experimental data reveal an exceedingly low success rate in TM perforation healing with detachment occurring in large numbers. It implies that the hydrophobic surface is not compatible to tissue and indirectly demonstrates a good performance in adhesion prevention. This may bring hope for the population frequently suffering from adhesive otitis media.

The hydrophilic surface is proven to have favorable tissue compatibility, which is manifested by the well repaired TM perforation and fused TM epithelial cells after 4 weeks of operation (Fig. 4). Fig. 4A and D show the perforated TM and TM for 4 weeks after the autologous fascia repair, respectively. Fig. 4B and E show the perforated TM and TM 4 weeks after the hydrophilic surface for repair, respectively. Fig. 4C shows the histology of TM after the autologous fascia repair (H&E staining, $100\times$ magnification). It could be seen that the TM is well covered with the epithelial cells on the fascia surface. Fig. 4F shows the histology of TM after the hydrophilic surface of JMs-22 for repair (H&E staining, $100\times$ magnification). One can see that the hydrophilic surface is also covered with epithelial cells.

Stenfors *et al.* thought that the period of TM perforation healing was about 7–14 days.[42] Santa Maria *et al.* suggested that it might
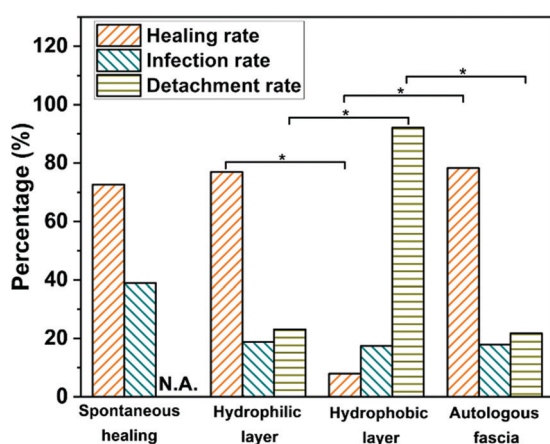

Fig. 3 Comparison of the healing rate, the infection rate, and the detachment rate of guinea pigs with TM perforations after spontaneous healing with the hydrophilic surface and the hydrophobic surface of JMs-22 and with the autologous fascia. Significance ($p < 0.5$) is suggested by the asterisk (*).
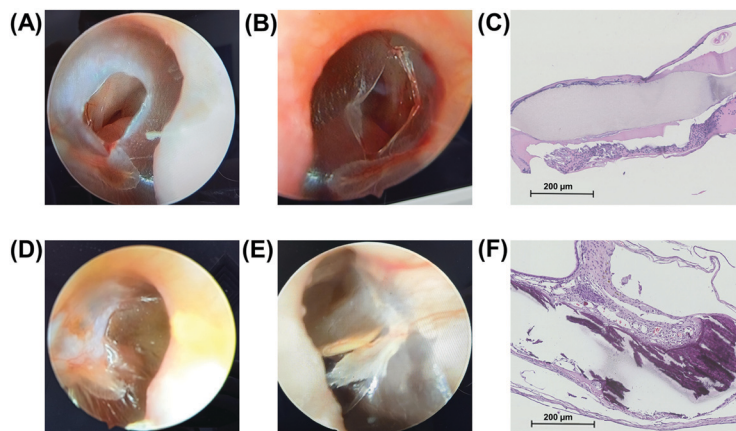
2724 | *J. Mater. Chem. B*, 2022, **10**, 2719–2727

This journal is © The Royal Society of Chemistry 2022

Fig. 4 (A and B) Perforated tympanic membrane. (D) TM after autologous fascia repair for 4 weeks (E) TM after repair for 4 weeks by the hydrophilic surface of JMs-22. (C) Histology of TM after autologous fascia repair, 100× magnification. (F) Histology of TM after repair for by the hydrophilic surface of JMs-22, 100× magnification.

take a longer time.[42] In clinical experience, the basic histological healing period is considered to be about 3–4 weeks. Of course, it shows certain differences between normal human individuals. Meanwhile, 4 weeks is enough for the histological healing after the myringoplasty with the autologous fascia material. Therefore, the guinea pigs after 4 weeks of repair were selected for the final experiment and monitored to have histological healing.

The normal TM shows a multilayer fiber structure consisting of the epidermal, lamina propria, and mucosal epithelial layers,

and is thick in the umbo while is thin around (Fig. S8, ESI†). The medial lamina propria is the thickest and one of the important components in the TM scaffold.[11] In our experiment, H&E staining was performed to observe the separated three-layer structure in a normal TM. Despite the moderate appearance and wide applications by many medical teams, autologous fascia is not perfect in perforation healing histologically. It is a pity that we could not find animal research on TM perforation repair using autologous fascia. This might be due to the difficulty in fascial
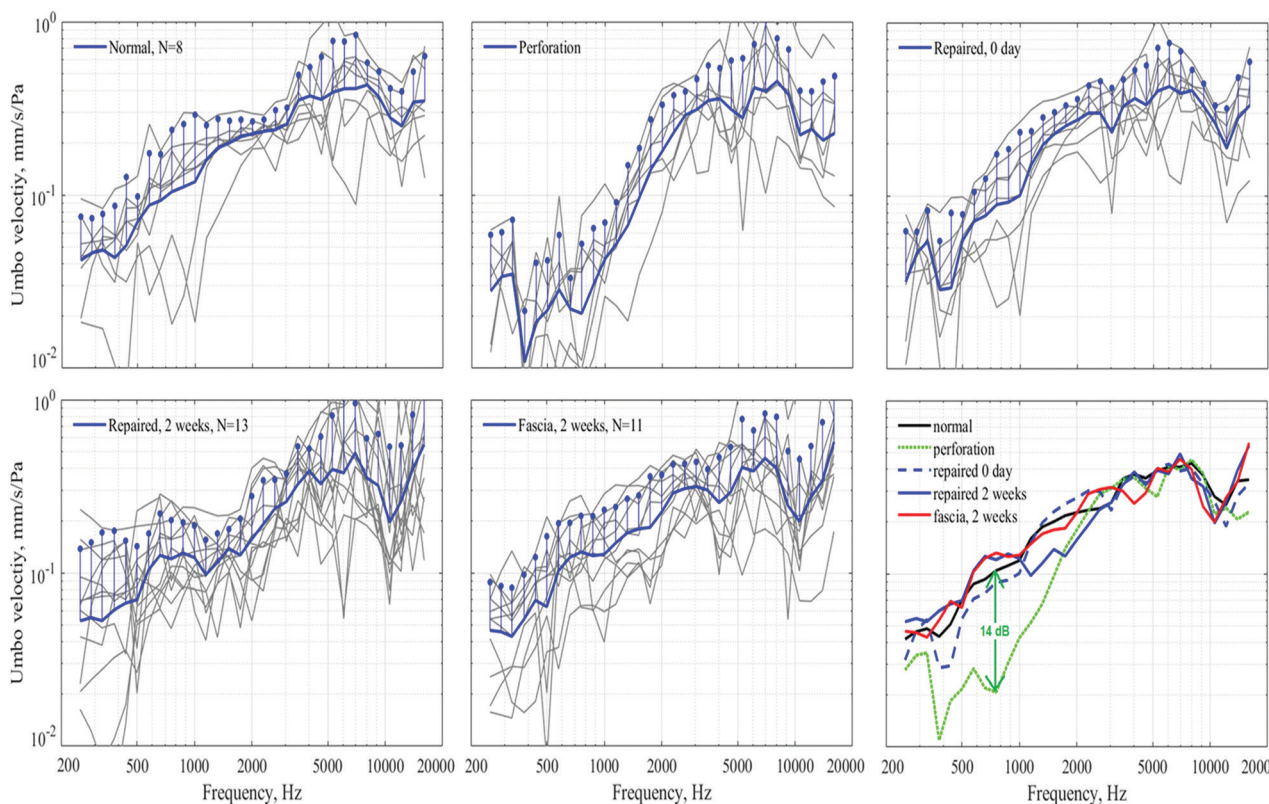

Fig. 5 Umbo velocities of TM of different states.

This journal is © The Royal Society of Chemistry 2022

J. Mater. Chem. B, 2022, **10**, 2719–2727 | **2725**

tissue extraction, which generally requires experienced senior ear surgeons. Moreover, from the TM tissue sections after repair, the distinctly stratified structure is present, where the mucosal cells on the inner layer and the epithelial cells on the outer layer grow well along the material scaffold with many cells better fused. Comparing our JMs-22 with the autologous fascia, the hydrophilic surface is superior in fusing with the residual TM, showing good reliability.

3.4 Laser Doppler vibrometer (LDV) measurements

The Laser Doppler vibrometer (LDV) measurements (Fig. 5) proved the favorable effect of our JMs-22 in instant acute TM healing. The persistent healing effect is also present 2 weeks later, resulting in vibration recovered to near normal. In our studies, tympanic perforation could be healed 10–14 days after repairment, known as clinical healing. Therefore, LDV was arranged 2 weeks after repair to obtain primary healing data, and a comparative analysis was conducted with the instant data after repair.

The human TM has a heterogeneous thickness with individual differences, generally ranging between 34 μm and 100 μm.[11,43–45] In this setting, JMs-22 was devised to have a similar thickness to the normal human TM. LDV, instead of auditory brainstem response audiometry (ABR), was selected as the main measurement means invalidating the healing performance and the mechanical properties of the applied material.[46] Reasons might also include that, ABR can be affected by multiple operations in animal experiments, leading to a higher incidence of data collection error, and it also fails to reflect the real material performance directly.

4 Conclusions

In summary, we have fabricated Janus membranes as novel synthetic implant materials for realizing the TM perforation repair and avoiding the postoperative adhesion simultaneously. These Janus membranes were prepared by the co-deposition of two biocompatible chemicals, TA and APTES, on polypropylene microfiltration substrates. The preparation process is fast, green, and low-cost. The Janus membranes can heal tympanic membrane perforation efficiently. The opposite wettability of the two surfaces leads to asymmetric cellular behaviors, which is proved by cell experiments and animal experiments. The Janus membranes are a burgeoning material for the TM perforation repair, which can not only heal the tympanic membrane perforation with their hydrophilic surface, but also possess the anti-adhesion properties via their hydrophobic surface.

Author contributions

Zhili Zhang: Methodology, formal analysis, resources, investigation, data curation and writing-original draft, visualization. Jin-Bo Li: Methodology, formal analysis, investigation, data curation and writing-original draft, visualization. Xu Li: Resources, investigation. Cheng-Ye Zhu: Validation and investigation. Liujie Ren: Formal analysis, investigation, data curation and visualization. Xiao-Jun

Huang: Conceptualization and supervision. Jian Wu: Supervision, project administration and funding acquisition. Jian Ji: Supervision, project administration and funding acquisition. Zhi-Kang Xu: Supervision, writing - review and editing, project administration and funding acquisition.

Conflicts of interest

There are no conflicts to declare.

Acknowledgements

References

1 F. L. Westphal, R. T. Sousa, L. C. Lima, L. C. Lima and S. Silva Mdos, *Braz. J. Otorhinolaryngol.*, 2013, **79**, 122.
2 J. S. Green, *Eye, Ear, Nose Throat Mon.*, 2017, **96**, 356.
3 Y. Matsuda, T. Kurita, Y. Ueda, S. Ito and T. Nakashima, *J. Laryngol. Otol.*, 2009, **123**, 81–89.
4 M. C. Ott and L. B. Lundy, *Postgrad. Med.*, 2001, **110**, 81–84.
5 C. Sagowski, P. Samuel, S. Wenzel and R. Leuwer, *HNO*, 2004, **52**, 720–723.
6 N. Hakuba, M. Iwanaga, S. Tanaka, Y. Hiratsuka, Y. Kumabe, M. Konishi, Y. Okanoue, N. Hiwatashi and T. Wada, *Otol. Neurotol.*, 2009, **31**, 118–121.
7 S. Kakehata, Y. Hirose, R. Kitani, K. Futai, S. Maruya, K. Ishii and H. Shinkawa, *Otol. Neurotol.*, 2008, **29**, 791–795.
8 S. Kanemaru, H. Umeda, Y. Kitani, T. Nakamura, S. Hirano and J. Ito, *Otol. Neurotol.*, 2011, **32**, 1218–1223.
9 B. Li, L. Zhou, M. Wang, Y. Wang and J. Zou, *Am. J. Otolaryngol.*, 2021, **42**, 102451.
10 E. D. Kozin and D. J. Lee, *Oper. Tech. Otolaryngol. Head Neck Surg.*, 2017, **28**, 2–10.
11 B. M. Teh, R. J. Marano, Y. Shen, P. L. Friedland, R. J. Dilley and M. D. Atlas, *Tissue Eng., Part B*, 2013, **19**, 116–132.
12 Z. C. Lou and J. G. He, *Clin. Otolaryngol.*, 2011, **36**, 221–226.
13 A. P. S. Immich, P. C. Pennacchi, A. F. Naves, S. L. Felisbino, R. L. Boemo, S. S. Maria-Engler and L. H. Catalani, *Mater. Sci. Eng., C*, 2017, **73**, 48–58.
14 G. Li, J. G. Feghali, E. Dinces, J. McElveen and T. R. Van De Water, *Arch. Otolaryngol., Head Neck Surg.*, 2001, **127**, 534–539.
15 J. Dornhoffer, *Laryngoscope*, 2003, **113**, 1844–1856.
16 A. A. Kolethekkat, R. Al Abri, K. Al Zaabi, N. Al Marhoobi, S. Jose, S. Pillai and J. Mathew, *J. Laryngol. Otol.*, 2018, **132**, 497–504.
17 E. H. Bedri, B. Korra, M. Redleaf and A. Worku, *Ann. Otol., Rhinol., Laryngol.*, 2019, **128**, 795–801.
18 Y. C. Hsu, C. L. Kuo and T. C. Huang, *J. Otolaryngol., Head Neck Surg.*, 2018, **47**, 44.
19 R. Bartel, M. Levorato, M. Adroher, S. Cardelus, A. Diaz, J. Lacima, C. Vazquez, A. Veneri, P. Wienberg, M. A. Claveria

and O. H. Haag, *Int. J. Pediatr. Otorhinolaryngol.*, 2019, **121**, 120–122.

20 J. Yang, H. N. Li, Z. X. Chen, A. He, Q. Z. Zhong and Z. K. Xu, *J. Mater. Chem. A*, 2019, **7**, 7907–7917.

21 H. C. Yang, W. Zhong, J. Hou, V. Chen and Z. K. Xu, *J. Membr. Sci.*, 2017, **523**, 1–7.

22 M. B. Wu, H. C. Yang, J. J. Wang, G. P. Wu and Z. K. Xu, *ACS Appl. Mater. Interfaces*, 2017, **9**, 5062–5066.

23 Z. Xiang, C. Z. Chu, H. Z. Xiang, C. Z. Chu, H. Xie, T. Xiang and S. B. Zhou, *ACS Appl. Mater. Interfaces*, 2021, **13**, 1463–1473.

24 B. Zhang, L. H. Jia, J. R. Jiang, S. S. Wu, T. Xiang and S. B. Zhou, *ACS Appl. Mater. Interfaces*, 2021, **13**, 36574–36586.

25 S. S. Wu, Z. J. Shao, H. Xie, T. Xiang and S. B. Zhou, *J. Mater. Chem. A*, 2021, **9**, 1048–1061.

26 C. Cui, T. Wu, X. Chen, Y. Liu, Y. Li, Z. Xu, C. Fan and W. Liu, *Adv. Funct. Mater.*, 2020, **30**, 2005689.

27 E. Prajatelistia, N. D. Sanandiya, A. Nurrochman, F. Marseli, S. Choy and D. S. Hwang, *Carbohydr. Polym.*, 2021, **251**, 117032.

28 H. Tsou, C. S. Wu, W. S. Hung, M. R. De Guzman, C. Gao, R. Y. Wang, J. Chen, N. Wan, Y. J. Peng and M. C. Suen, *Polymer*, 2019, **160**, 265–271.

29 S. M. Bai, X. L. Zhang, X. L. Lv, M. Y. Zhang, X. W. Huang, Y. Shi, C. H. Lu, J. B. Song and H. H. Yang, *Adv. Funct. Mater.*, 2020, **30**, 1908381.

30 S. Kuddannaya, J. Bao and Y. Zhang, *ACS Appl. Mater. Interfaces*, 2015, **7**, 25529–25538.

31 Y. S. Kara and S. Yalduz, *J. Mol. Struct.*, 2019, **1193**, 158–165.

32 N. Faucheux, R. Schweiss, K. Lutzow, C. Werner and T. Groth, *Biomaterials*, 2007, **25**, 2721–2730.

33 S. J. Lee, G. Khang, Y. M. Lee and H. B. Lee, *J. Colloid Interface Sci.*, 2003, **259**, 228–235.

34 T. Kawauchi, *Int. J. Mol. Sci.*, 2012, **13**, 4564–4590.

35 T. Xiang, J. W. Hou, H. Xie, X. Liu, T. Gong and S. B. Zhou, *Nano Today*, 2020, **35**, 100980.

36 Y. Arima and H. Iwata, *Biomaterials*, 2007, **28**, 3074–3082.

37 V. Antonini, S. Torrengo, L. Marocchi, L. Minati, M. Dalla Serra, G. Bao and G. Speranza, *Colloids Surf., B*, 2014, **113**, 320–329.

38 D. E. Weber, M. T. Semaan, J. K. Wasman, R. Beane, L. J. Bonassar and C. A. Megerian, *Laryngoscope*, 2006, **116**, 700–704.

39 W. Q. Wang, Z. M. Wang and F. L. Chi, *Acta Oto-Rhino-Laryngol. Belg.*, 2004, **124**, 1141–1144.

40 A. Golz, D. Goldenberg, A. Netzer, M. Fradis, S. T. Westerman, L. M. Westerman and H. Z. Westerman, *Head Neck Surg.*, 2003, **128**, 565–570.

41 L. E. Stenfors, B. Salen and B. Winblad, *Acta Oto-Rhino-Laryngol. Belg.*, 1980, **90**, 267–274.

42 P. L. Santa Maria, M. D. Atlas and R. Ghassemifar, *Wound Repair Regen.*, 2007, **15**, 450–458.

43 Y. Shen, S. L. Redmond, B. M. Teh, S. Yan, Y. Wang, L. Zhou, C. A. Budgeon, R. H. Eikelboom, M. D. Atlas, R. J. Dilley, M. Zheng and R. J. Marano, *Tissue Eng., Part A*, 2013, **19**, 657–668.

44 R. M. Baxter, T. Dai, J. Kimball, E. Wang, M. R. Hamblin, W. P. Wiesmann, S. J. McCarthy and S. M. Baker, *J. Biomed. Mater. Res., Part A*, 2013, **101**, 340–348.

45 E. E. Altuntas and Z. Sumer, *Arch. Oto-Rhino-Laryngol.*, 2013, **270**, 81–86.

46 D. Schwarz, D. Pazen, K. Gosz, S. Schwarz, M. Nunning, A. O. Gostian, L. Koerber, R. Breiter, N. Rotter and D. Beutner, *Otol. Neurotol.*, 2016, **37**, 692–697.

This journal is © The Royal Society of Chemistry 2022

J. Mater. Chem. B, 2022, **10**, 2719–2727 | 2727